FUDMA Journal of Sciences (FJS)
ISSN online: 2616-1370
ISSN print: 2645 - 2944
Vol. 10 No. 16, June, 2026, pp 688 – 692
DOI: https://doi.org/10.33003/fjs-2026-1016-5862

Monte Carlo Investigation of the Attenuation Characteristics of Granite Doped with Palm Kernel Shell Ash

***Abako Bethel Keghtor, Abdullahi Abubakar Mundi and Mohammed Mustapha Idris**

Department of Physics, Nasarawa State University Keffi, Nasarawa State, Nigeria.

*Corresponding authors' email: bethelabakokeghtor@gmail.com

ABSTRACT

Radiation shielding materials that combine effective attenuation with environmental sustainability are increasingly being investigated as alternatives to conventional shielding materials. This study investigates the gamma-ray attenuation characteristics of granite doped with palm kernel shell ash (PKSA) using Monte Carlo simulation with the Tool for Particle Simulation (TOPAS), based on the Geant4 platform. Six composite samples (M1–M6), containing 0, 20, 40, 60, 80, and 100 wt.% PKSA, were investigated at photon energies of 0.015, 0.050, 0.100, 0.300, 0.662, and 1.500 MeV, with 1,000,000 photon histories used for each simulation. The linear attenuation coefficient (LAC) and mass attenuation coefficient (MAC) were calculated from the Beer–Lambert relation. Both LAC and MAC decreased noticeably with increasing photon energy for all samples, with the largest reduction occurring between 0.015 and 0.050 MeV. This behaviour mainly reflects the strong contribution of the photoelectric effect at low photon energies, while Compton scattering becomes increasingly important at higher energies. The attenuation coefficients generally increased with increasing PKSA content, with M6 exhibiting the highest LAC and MAC values, particularly at low photon energies. The differences among the composites became smaller at higher photon energies. At 0.015 MeV, the LAC ranged from 19.8370 to 25.1180 cm^{-1}, while the MAC ranged from 7.3470 to 9.2007 $cm^2 g^{-1}$ across M1–M6. The results indicate that PKSA incorporation can improve the photon attenuation characteristics of granite-based composites, particularly at low photon energies.

Received: 01 Sep. 2026

Accepted: 03 Sep. 2026

Published: 12 Sep. 2026

Keywords: Granite, Palm Kernel Shell Ash, Gamma-Ray Attenuation, Monte Carlo Simulation, TOPAS, Radiation Shielding

INTRODUCTION

Radiation shielding is essential, especially when protection from ionizing radiation is required. Lead and concrete are traditionally used for this purpose because of their high density and ability to attenuate radiation. Nevertheless, concerns about toxicity, weight, and environmental impact have driven the development of alternative shielding materials that are safer and more environmentally sustainable (Zeng et al., 2023).

Granite, a hard igneous rock, possesses inherent radiation-shielding properties and has been investigated as a potential shielding material. Incorporating palm kernel shell ash (PKSA), an agricultural by-product containing elements such as silica, alumina, and iron oxides associated with photon attenuation, can modify its attenuation characteristics (Najam et al., 2016). Using palm kernel shell ash (PKSA) also offers an opportunity to turn agricultural waste into shielding composites. Agro-waste derived ash has already shown promise in this role elsewhere, rice husk ash has been used as a low-cost silica source in lead-free glass systems that achieve lower half-value layers than commercial shielding glass (Annadurai et al., 2026), and industrial bottom ash has been shown to raise the gamma attenuation efficiency of recycled polymer composites by up to 74% at modest filler loadings (Zadeh et al., 2025). These studies support agro- and industrial-waste ash as a viable shielding filler in general, but palm kernel shell ash specifically, combined with granite, has not been examined this way.

Monte Carlo simulation provides a suitable approach for studying photon transport and attenuation in complex materials. The Tool for Particle Simulation (TOPAS), developed on the Geant4 platform, enables the modelling of radiation transport and material interactions under defined irradiation conditions (Mansouri et al., 2020). Computational determination of shielding parameters such as LAC, MAC, HVL, and MFP is similarly well established for other material systems; for instance, Geidam and Abdulsalam (2026) used Phy-X/PSD software to show that increasing BaO content in borosilicate glass steadily reduced HVL and MFP, confirming that composition-driven shifts in shielding performance can be reliably captured without fabricating physical samples. Despite growing interest in alternative shielding materials, the shielding characteristics of granite–palm kernel shell ash (PKSA) composites remain insufficiently studied, particularly the effect of composition on photon attenuation.

Therefore, this study investigates the attenuation characteristics of granite– palm kernel shell ash (PKSA) composites using Monte Carlo simulation with the TOPAS code.

MATERIALS AND METHODS

Materials

This study used granite and palm kernel shell ash (PKSA) as the primary materials. We examined six composite samples, labelled M1 to M6, corresponding to 0, 20, 40, 60, 80, and 100 wt. % palm kernel shell ash incorporated into granite. The elemental compositions of the granite and of the palm kernel shell ash (PKSA) were taken from Ugbe et al. (2016) and Ajayi et al. (2019), respectively. We used the average compositions and densities in TOPAS, with the elemental mass fractions specified for each composite as shown in the table 1. The elemental mass fractions of the composites were obtained by combining the elemental mass fractions of granite and palm kernel shell ash according to their respective weight percentages, using the relation:

$$w_{i,c} = (1 - x)w_{i,g} + xw_{i,p} \quad (1)$$

Where $w_{i,c}$is the mass fraction of element $i$in the composite, $w_{i,g}$ and $w_{i,p}$ are the corresponding mass fractions in granite and palm kernel shell ash, respectively, and x is the mass fraction of palm kernel shell ash in the composite.

Table 1: Elemental Composition and Density of the Granite- Palm Kernel Shell Ash Composites Used in the TOPAS Simulations

Sample	O	Si	Al	K	Na	Ca	Fe	Mg	Ti	P	Density (g/cm³)
M1	0.48547	0.33656	0.07410	0.04151	0.02597	0.01072	0.01399	0.00603	0.00480	0.00087	2.70
M2	0.47990	0.32534	0.07304	0.04151	0.02077	0.03216	0.01189	0.01086	0.00384	0.00070	2.71
M3	0.47434	0.31412	0.07198	0.04151	0.01558	0.05360	0.00979	0.01568	0.00288	0.00052	2.71
M4	0.46878	0.30290	0.07092	0.04151	0.01039	0.07504	0.00769	0.02050	0.00192	0.00035	2.71
M5	0.46322	0.29168	0.06986	0.04151	0.00519	0.09648	0.00560	0.02533	0.00096	0.00018	2.71
M6	0.45765	0.28046	0.06880	0.04151	0.00000	0.11792	0.00350	0.03015	0.00000	0.00000	2.73

Methods

Topas Monte Carlo Simulation

Monte Carlo simulation used the Tool for Particle Simulation (TOPAS), which is a simulation platform built on the Geant4 toolkit. TOPAS allows you to set the geometry, material makeup, source features, physics processes, and scoring conditions needed for particle transport simulations (Perl et al., 2012; Schümann et al., 2012; Faddegon et al., 2020).

A parallel monoenergetic gamma-ray beam was used as the radiation source. The energies of the six photons studied were 0.015, 0.050, 0.100, 0.300, 0.662 and 1.500 MeV. The source was placed 20 cm in front of the shielding material and aimed along the positive z-axis. In each simulation, 1,000,000 photon histories were employed. The statistical uncertainty associated with the transmitted photon counts was estimated from Poisson counting statistics using;

$$\frac{1}{\sqrt{N_t}} \quad (2)$$

Where N_t is the number of transmitted photons. The relative uncertainty ranged from approximately 0.11% to 0.35% across the simulations.

The beam had no energy spread and no angular spread. The shielding material was represented as a square slab with a cross section of 10 cm × 10 cm. The half-length of the shielding geometry in the beam direction was varied manually by photon energy: 0.05 cm at 0.015 MeV, 0.10 cm at 0.050 MeV, 0.25 cm at 0.100 MeV, 0.50 cm at 0.300 MeV, 2.50 cm at 0.662 MeV, and 5.00 cm at 1.500 MeV. Since TOPAS specifies the box size by half-length, the actual physical thickness of the absorber along the beam direction was twice this half-length, and this physical thickness was used in the Beer–Lambert calculation.

Table 2: The Photon Energies, Shielding Thicknesses and Photon Histories Employed In the TOPAS Simulations

Photon Energy (MeV)	Half-length shield thickness (cm)	Histories
0.015	0.05	1,000,000
0.050	0.10	1,000,000
0.100	0.25	1,000,000
0.300	0.50	1,000,000
0.662	2.50	1,000,000
1.500	5.00	1,000,000

The Penelope electromagnetic physics model was used for photon and electron transport, and it included fluorescence, Auger emission, and Auger-cascade processes. The incident and transmission detectors were placed before and after the shielding material, respectively. The detector planes are modeled as thin volumes of vacuum.

The SurfaceTrackCount quantity recorded both incident and transmitted gamma photons. Only gamma particles were taken into account in this scoring, and those photons which travelled into the appropriate detector surfaces were counted. The number of incident photons was measured at the entrance detector, and that of the transmitted photons was recorded at the transmission detector. The photon transmission through each composite was calculated from:

$$T = \frac{I}{I_0} \quad (3)$$

Where I_0 represents the intensity of the incident photons and I the intensity of the transmitted photons.

The linear attenuation coefficient (LAC) was calculated using the Beer-Lambert relation (Farokhzad et al., 2021):

$$\mu = -\frac{1}{x}\ln\left(\frac{I}{I_0}\right) \quad (4)$$

Where μ denotes the linear attenuation coefficient (cm⁻¹), x is the thickness of the shielding (cm), I_0 is the intensity of the incident photons, and I is the intensity of the transmitted photons.

The mass attenuation coefficient (MAC) was calculated from the linear attenuation coefficient and the density of each composite according to the equation (Farokhzad et al., 2021):

$$\mu_m = \frac{\mu}{\rho} \quad (5)$$

The mass attenuation coefficient μ_m is measured in $cm^2\ g^{-1}$, μ denotes the linear attenuation coefficient in cm^{-1}, and ρ is the density of the composite in $g\ cm^{-3}$.

The simulation results were processed and compiled into a table using Microsoft Excel. The calculated LAC and MAC values were then compared for the six granite-palm kernel shell ash composites across the photon-energy range. Graphs were created from the calculated values using OriginPRO2026b, showing how attenuation coefficients varied with photon energy and comparing the shielding properties of the different composite compositions.

RESULTS AND DISCUSSION

Linear Attenuation Coefficient (LAC)

Table 3 shows the calculated linear attenuation coefficient for 0.015, 0.050, 0.100, 0.300, 0.662 and 1.5 MeV.

Table 3: Calculated Linear Attenuation Coefficient for Granite-Palm Kernel Shell Ash Composite.

	LAC (cm^{-1})					
Energy (MeV)	**M1**	**M2**	**M3**	**M4**	**M5**	**M6**
0.015	19.8370	21.1021	22.0643	23.0232	23.9961	25.1180
0.050	0.8833	0.9890	1.0155	1.0420	1.0691	1.1046
0.100	0.3989	0.4550	0.4583	0.4616	0.4650	0.4716
0.300	0.2358	0.2805	0.2807	0.2810	0.2812	0.2834
0.662	0.1970	0.1978	0.1979	0.1980	0.1981	0.1996
1.500	0.1233	0.1239	0.1239	0.1240	0.1241	0.1251

Figure 1 shows the relationship between photon energy and the linear attenuation coefficient (LAC) for the six granite-palm kernel shell ash composite samples.

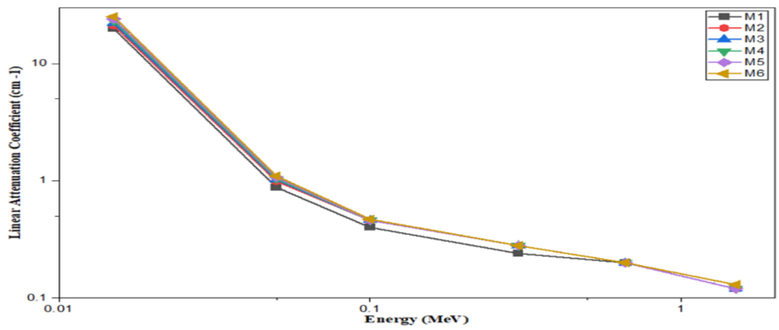

Figure 1: LAC vs Photon Energy for six granite-palm kernel shell ash composite samples

For all samples, the LAC decreases considerably as photon energy increases. The most marked decrease occurs from 0.015 to 0.050 MeV, after which the curve levels off gradually. The highest LAC values are found at 0.015 MeV, the lowest at 1.50 MeV, and M6 has the highest LAC while M1 has the lowest. When the energy is 0.015 MeV, the LAC rises from 19.8370 cm^{-1} for M1 to 25.1180 cm^{-1} for M6; at higher energies, however, this difference is much smaller, with the values at 0.662 MeV lying between 0.1970 and 0.1996 cm^{-1} and those at 1.50 MeV lying between 0.1233 and 0.1251 cm^{-1}. The significant decrease at low photon energy is mainly due to the photoelectric effect, and the interaction probability in this region drops rapidly as photon energy increases. As photon energy increases, Compton scattering becomes increasingly important, causing the attenuation coefficients to decrease and cluster more closely.

This pattern agrees with earlier research on granite-based shielding materials. Najam et al. (2016) found that the attenuation coefficient of granite decreases progressively as the photon energy increases. The current LAC values at about 0.662 MeV are also similar to those obtained from published granite data using XCOM (Berger et al., 2010), although differences are expected because the present samples are granite palm kernel shell ash composites with different compositions and densities (Elsafi et al., 2021). This comparison validates the pure granite endpoint (M1, 0% PKSA), since the published reference data are for granite rather than the granite–PKSA composites.

Mass Attenuation Coefficient (MAC)

Table 4 shows the calculated mass attenuation coefficient for 0.015, 0.050, 0.100, 0.300, 0.662 and 1.5 MeV.

Table 4: Calculated Mass Attenuation Coefficient for Granite-Palm Kernel Shell Ash Composite

MAC (cm^2/g)						
Energy (MeV)	**M1**	**M2**	**M3**	**M4**	**M5**	**M6**
0.015	7.3470	7.7868	8.1418	8.4644	8.8221	9.2007
0.050	0.3272	0.3649	0.3747	0.3831	0.3931	0.4046
0.100	0.1477	0.1679	0.1691	0.1697	0.1710	0.1727
0.300	0.0873	0.1035	0.1036	0.1033	0.1034	0.1038
0.662	0.0730	0.0730	0.0730	0.0728	0.0728	0.0731
1.500	0.0457	0.0457	0.0457	0.0456	0.0456	0.0458

Figure 2 shows the mass attenuation coefficient (MAC) in relation to photon energy for the six granite–PKSA composites.

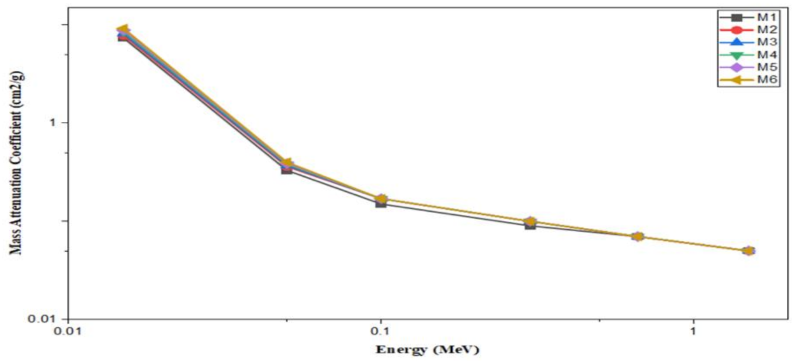

Figure 2: MAC vs Photon Energy for six granite-palm kernel shell ash samples.

For all samples, the mass attenuation coefficient decreases as photon energy increases, with the highest values at 0.015 MeV and the lowest at 1.50 MeV. At 0.015 MeV, the MAC rises from about 7.3470 cm² g⁻¹ for M1 to 9.2007 cm² g⁻¹ for M6; however, at 0.050 MeV it drops to between 0.3272 and 0.4046 cm² g⁻¹, and at 0.662 MeV it is about 0.0730 cm² g⁻¹. The sharp drop observed at low photon energy is mainly due to photoelectric absorption, whereas the growing role of Compton scattering at higher photon energies causes the gradual decrease in the MAC.

The current results agree with the general behaviour previously observed for granite based on experimental measurements and XCOM calculations. Elsafi et al. (2021) gave XCOM MAC values of about 0.0764–0.0769 cm² g⁻¹ at 0.6617 MeV for granite samples, whereas the present study obtained values of approximately 0.0730–0.0731 cm² g⁻¹. The discrepancy is relatively small because the materials examined differ. Najam et al. (2016) also found that the MAC decreased as the photon energy increased for granite. The higher MAC value for M6 at low photon energies shows that, as the amount of palm kernel shell ash increases, the composite's attenuation properties improve in this energy range. At higher energies, the differences between samples decrease, meaning the effect of composition on photon attenuation in that region is reduced.

CONCLUSION

The Monte Carlo simulation showed that as the photon energy increased, both the linear attenuation coefficient (LAC) and the mass attenuation coefficient (MAC) of the granite palm kernel shell ash composites decreased. Generally, the attenuation coefficients increased with increasing PKSA content, with the highest values in M6, especially at low photon energies. The differences between the various composites became less significant at higher photon energies. These results show that increasing PKSA content generally improves the gamma-ray attenuation characteristics of the composites, particularly at low photon energies, suggesting it could serve as a potential material for radiation shielding applications. An experimental investigation of the fabricated granite–palm kernel shell ash composite is recommended to validate the simulated attenuation characteristics under controlled irradiation.

REFERENCES

Ajayi A. S., Oluwoye J., Olutoge F. A., & Coker A. O. (2019). “impact of palm kernel shell ash (pksa) on the strength and water absorption properties of earth blocks.” *ASJ International Journal of Advances in Scientific Research and Reviews (IJASRR)* 04(03), 129-135. https://www.researchgate.net/publication/383125451

Annadurai, G., Chaiphaksa, W., Mutuwong, C., Yonphan, S., Ruangtaweep, Y., Cheewasukhanont, W., Intachai, N., Tungjai, M., Kothan, S., Kim, H. J., & Kaewkhao, J. (2026). Lead-free glass for radiation shielding application by utilizing agricultural waste material: Organ-specific effective dose rate estimation. *Radiation Physics and Chemistry, 238*, 113137. https://doi.org/10.1016/j.radphyschem.2025.113137

Berger, M. J., Hubbell, J. H., Seltzer, S. M., Chang, J., Coursey, J. S., Sukumar, R., Zucker, D. S. & Olsen, K. (2010) *XCOM: Photon cross sections database (Version 1.5).* National Institute of Standards and Technology. https://doi.org/10.18434/T48G6X

Elsafi, M., Alrashedi, M. F., Sayyed, M. I., Al-Hamarneh, I. F., El-Nahal, M. A., El-Khatib, M., Khandaker, M. U., Osman, H., & Askary, A. E. (2021). The Potentials of Egyptian and Indian Granites for Protection of Ionizing Radiation. *Materials*, *14*(14), 3928. https://doi.org/10.3390/ma14143928

Faddegon, B., Ramos-Méndez, J., Schuemann, J., McNamara, A., Shin, J., Perl, J., & Paganetti, H. (2020). The TOPAS tool for particle simulation, a Monte Carlo simulation tool for physics, biology and clinical research. *Physica Medica*, *72*, 114–121. https://doi.org/10.1016/j.ejmp.2020.03.019

Farokhzad, R., Dadashi, A., & Sohrabi, A. (2021). Ferrophosphorus aggregates shielding properties on heavy concrete exposed to gamma rays from a caesium-137 source. *Cement Wapno Beton*, *26*(4), 307–322. https://doi.org/10.32047/CWB.2021.26.4.4

Geidam, I. G., & Abdulsalam, H. (2026). Simulation of gamma radiation shielding parameters of borosilicate glass using Phy-X/PSD software. *FUDMA Journal of Sciences, 10*(13), 49–54. https://doi.org/10.33003/fjs-2026-1013-5561

Mansouri, E., Mesbahi, A., Malekzadeh, R., & Mansouri, A. (2020). Shielding characteristics of nanocomposites for protection against X- and gamma rays in medical applications: Effect of particle size, photon energy and nano-particle concentration. *Radiation and Environmental Biophysics*, *59*(4), 583–600. https://doi.org/10.1007/s00411-020-00865-8

Najam, L. A., Hashim, A. K., Ahmed, H. A., & Hassan, I. M. (2016). Study the Attenuation Coefficient of Granite to Use It as Shields against Gamma Ray. *Detection*, *04*(02), 33–39. https://doi.org/10.4236/detection.2016.42005

Perl, J., Shin, J., Schümann, J., Faddegon, B., & Paganetti, H. (2012). TOPAS: An innovative proton Monte Carlo platform for research and clinical applications. *Medical Physics*, *39*(11), 6818–6837. https://doi.org/10.1118/1.4758060

Schümann, J., Paganetti, H., Shin, J., Faddegon, B., & Perl, J. (2012). Efficient voxel navigation for proton therapy dose calculation in TOPAS and Geant4. *Physics in Medicine and Biology*, *57*(11), 3281–3293. https://doi.org/10.1088/0031-9155/57/11/3281

Ugbe, F. C., Adiela, U.-P., & Ebegbare, U. C. (2016). Major and Trace Element Geochemistry of Granites in Koji, Kogi State, Nigeria. *Research Journal of Environmental and Earth Sciences*, *8*(1), 8–12. https://doi.org/10.19026/rjees.8.2697

Zadeh, K. M., Al-Ejji, M., Ponnamma, D., Abdulmalik, D. A., Iqbal, F., Hasnawi, D., Azoz, A., & Irshidat, M. (2025). Valorizations of recycled polymers/bottom ash composite for gamma attenuation and radiation shielding application. *Scientific Reports*, *15*, 40817. https://doi.org/10.1038/s41598-025-24552-0

Zeng, C., Kang, Q., Duan, Z., Qin, B., Feng, X., Lu, H., & Lin, Y. (2023). Development of Polymer Composites in Radiation Shielding Applications: A Review. *Journal of Inorganic and Organometallic Polymers and Materials*, *33*(8), 2191–2239. https://doi.org/10.1007/s10904-023-02725-6